ELSEVIER

Applied Surface Science 187 (2002) 218–234

applied surface science

www.elsevier.com/locate/apsusc

Surface topography of gibbsite crystals grown from aqueous sodium aluminate solutions

C. Sweegers[a], M. Plomp[a], H.C. de Coninck[a], H. Meekes[a], W.J.P. van Enckevort[a,*], I.D.K. Hiralal[b], A. Rijkeboer[b]

[a]*Faculty of Science, RIM Department of Solid State Chemistry, Research Institute for Materials, University of Nijmegen, Toernooiveld 1, 6525 ED Nijmegen, The Netherlands*

[b]*Billiton Aluminium B.V., Mariahoeveplein 6, 2591 TV The Hague, The Netherlands*

Received 3 September 2001; accepted 14 November 2001

Abstract

Optical, scanning electron and atomic force microscopy were used to examine the surface topography of gibbsite (γ-$Al(OH)_3$) crystals grown from supersaturated caustic soda solutions. Several growth phenomena like monomolecular and higher steps, growth hillocks, contact nucleation of steps and planar faults were observed. It turned out that the growth features observed are related to the defect structures of the different gibbsite crystal morphologies found. Single crystalline lozenges of a few μm thickness have hillocks on the basal {0 0 1} faces, which are related to one or a few dislocations. For ultrathin lozenges (few tens of nm thick and an aspect ratio larger than 1000), the surface morphology is flawless and no dislocation sources emerging the {0 0 1} surface were found. Here growth proceeds by 2D nucleation. The second type of crystals, sixfold twinned hexagons, has irregular {0 0 1} surfaces as a result of many defects. The introduction of defects leads to enhanced growth parallel to the *c*-axis. Lateral expansion proceeds by a 2D nucleation of the fast growing {1 0 0} side faces and the enhanced 2D nucleation at the re-entrant corners at the outcrops of twin planes. Crystals of the third major crystal morphology found, i.e. prisms, also exhibit many defects. Mosaicity was observed and related to the presence of misaligned crystallites or impurities. The fact that the prismatic crystals do not show a pronounced lateral growth as the hexagons do, suggests that besides defects also other factors influence gibbsite crystal growth.

PACS: 68.35.Bs; 68.37.Ps; 81.10.-h; 81.10.Du

Keywords: Gibbsite; $Al(OH)_3$; Atomic force microscopy; Surface morphology; Defects; Crystal growth mechanisms

1. Introduction

The crystallisation of gibbsite, γ-$Al(OH)_3$, from Bayer liquors as applied in the aluminium industry has been widely studied in the last few decades. Most of the previous work considered crystallisation kinetics and agglomeration using batch crystallisers and was especially focused on the influence of the most important parameters—like caustic concentration, supersaturation, seeds and impurities—on the crystallisation rate [1–16]. Only a few studies reported on surface topography and its relation to the growth mechanism of gibbsite [17–23]. The investigation of

* Corresponding author. Tel.: +31-24-3653433; fax: +31-24-3653067.
E-mail address: wvenck@sci.kun.nl (W.J.P. van Enckevort).

0169-4332/02/$ – see front matter
PII: S0169-4332(01)00995-3

the surface structure is of high interest, because crystallisation processes take place at the surface.

Already starting from 1959, optical and scanning electron microscopy (SEM) were used to examine the polycrystallinity of gibbsite [17–19]. It was concluded that twinning, coherent internal boundaries and plate-like branches lead to the polycrystallinity of gibbsite crystals under industrial growth conditions. It was suggested that the formation of plate-like branches on the {0 0 1} basal plane in particular is the result of surface nuclei poorly oriented by dislocations in the underlying crystal. The initial orientation imposed by these defects determine the preferred orientation of the subsequently growing crystallites. Many crystals grew out to agglomerates in this way.

In 1972, Brown [20] examined the changes in surface topography of gibbsite crystals during crystallisation using SEM. At high supersaturations of 150%, the basal surfaces of gibbsite showed a wave-like pattern, which was interpreted as terraces or steps growing over the surface. Only a few straight steps were observed. As crystal growth continued, the supersaturation decreased and surface irregularities were smoothed out. At low supersaturation (25%), the crystallisation rate became negligibly small. They concluded that the crystal growth of gibbsite under Bayer process conditions occurs by a 2D nucleation mechanism with little or no contribution from screw dislocations.

Recently, Lloyd et al. [21] used ex situ atomic force microscopy (AFM) to image the surface of gibbsite crystals. Most surfaces of the crystals were covered with small {0 0 1} plates tilted at an angle with respect to the underlying basal face. The surfaces of these plates were rough. The author suggested that growth of gibbsite is related to a mechanism dominated by the spreading of these layers.

AFM studies by Freij et al. [22] showed the presence of various defects on the basal face of gibbsite, which might influence the crystal growth processes. At low supersaturation growth occurred by step growth from polygonal growth hillocks. At high supersaturation, circular nuclei were observed, developing into elongated features which coalesced to form a smooth surface. The authors suggested a continuous birth and spread mechanism. Under the same experimental conditions also step growth from a growth hillock was observed.

In a previous paper [24], using optical and electron microscopy, we have distinguished three main types of gibbsite crystals, namely (1) large plate-like hexagons, (2) lozenges and (3) prisms (rod-shaped crystals). Polarisation microscopy showed that the large hexagons are sixfold twinned in {1 1 0}, while the lozenges are single crystalline. The prisms showed various forms of twinning. Besides these three main categories, other shapes of gibbsite crystals were observed in batches grown from similar Bayer liquors. Examples are truncated lozenges and block-shaped crystals, intermediate between plates and prisms. It is to be expected that the different habits of gibbsite crystals are related to different growth mechanisms. A detailed investigation of the crystal surface topography can give more information about the growth properties of these habits.

In this paper, the results of ex situ microscopic studies of the surface structure of gibbsite crystals in relation to their defect structure are reported. In this, special attention is focused on the differences between the three main morphologies of gibbsite.

2. Experimental

Gibbsite crystals used for investigation of the surface topography are nucleated and grown from pure aqueous sodium aluminate–sodium hydroxide liquors, referred to as Bayer liquors. The solutions are prepared as described elsewhere [24]. The Bayer liquors used are composed of 6 and 4 M NaOH with a relative gibbsite supersaturation of 0.63 and 0.67, respectively [25]. In the North American industries terminology, these liquor compositions correspond to a sodium or caustic concentration of $C = 300$ and 200 g/l Na_2CO_3 and an alumina to caustic concentration ratio, $A/C = 0.8$ and 0.65 (g/l Al_2O_3/g/l Na_2CO_3), respectively. The liquors were poured in Teflon vessels, placed in a thermostatic bath of 80 °C under gentle stirring conditions and allowed to crystallise during 24 h.

Special attention was paid to the collection of the crystallised particles from the solution in such a way that artefacts formed during separation from the solution were minimal. In case of a shut-off effect, the nature and extent of the changes to the surface morphology will obscure information about the actual

growth processes. Therefore, prior to collection the solutions were diluted with sodium hydroxide solution of volume, concentration and temperature identical to the original Bayer liquors. This stopped the growth process. Subsequently, the solutions were filtered through a Millipore HVLP filter (45 μm) and washed with hot deionised water.

As will be described in Section 3, gibbsite crystals with a large variety in habit and size were obtained, even in a single experiment. The crystals were regularly checked with X-ray powder diffraction (XPD) and Raman spectroscopy to verify whether pure gibbsite was formed and not one of the other aluminium (oxide) hydroxide polymorphs. The bulk analyses using XPD as well as analyses of individual crystals using Raman spectroscopy always identified gibbsite to be the only polymorph.

Single crystals different in habit and size were collected on sample holders. The crystal surface topography was examined using differential interference contrast microscopy (DICM), SEM (Jeol T-300 and high-resolution Jeol 600F) and AFM (Topometrix TMX 2000 and Digital Instruments Dimension 3100). The AFMs operated in contact mode using silicon nitride cantilevers. The crystals selected for AFM observations had relatively smooth surfaces as imaged by DICM, to minimise any scan problems. The defect structure and twinning of the crystals were investigated by using optical transmission polarisation microscopy.

3. Results and discussion

3.1. Gibbsite crystal morphologies

Gibbsite is the most common polymorph of aluminium trihydroxide. It has a monoclinic space group, $P2_1/n$, with $a = 8.684$ Å, $b = 5.078$ Å, $c = 9.736$ Å and $\beta = 94.54°$ [26,27]. The structure of gibbsite is pseudohexagonal with the *c*-axis as the pseudohexagonal axis. The morphology of natural gibbsite crystals is usually reported as pseudohexagonal plate-like with {0 0 1} basal, and {1 0 0} and {1 1 0} side faces [27,28].

The crystallisation experiments of gibbsite from caustic sodium aluminate solutions resulted in crystals of different shapes and sizes. The variation in crystal habit and size within one batch was in most cases larger than that between two batches at different growth conditions. This strongly indicates that the defect properties of the individual crystals are more important than the imposed growth conditions. Despite this variation in shapes, the three main morphologies, lozenges, hexagons and prisms, could be identified well.

Crystalline material grown from sodium aluminate solutions of $C = 300$ g/l Na_2CO_3 and $A/C = 0.8$ at 80 °C ($\sigma = 0.63$) mostly consisted of hexagonal crystals, up to 100 μm in diameter and 15 μm thick. An example is shown in Fig. 1a. The optical polarisation micrograph of such a hexagon shows sixfold twinning (Fig. 1b). The morphology of hexagons and their twin characteristics have already been described in Ref. [24], where the twin boundaries have been identified as {1 1 0} and the side faces as {1 0 0}. This regular twinning was observed for all hexagons, often resulting in crystals having a convex top and a concave bottom face (see also Ref. [24]). The hexagons were sometimes more block-shaped, with smaller lateral dimensions, resulting in an aspect ratio close to 1.

Figs. 1c and d show lozenge-shaped crystals which were also found in these batches. It was shown by polarisation microscopy that the lozenges are single crystalline, with {0 0 1} basal and {1 1 0} side faces. Two types of lozenges could be distinguished: *thicker* lozenges of 30–50 μm in diameter and 5–7 μm thick (Fig. 1c) and *ultrathin* lozenges of 10–30 μm in diameter and only 20–50 nm thick (Fig. 1d).

Under growth conditions of $C = 200$ g/l Na_2CO_3, $A/C = 0.65$ and $T = 80$ °C ($\sigma = 0.67$), similar twinned hexagons and lozenges were obtained. However, the most dominant species in these batches were block-shaped crystals, with sizes typically 10 μm in diameter and 10 μm thick (Fig. 1e). These blocks had also twinning in {1 1 0} and, in addition, twinning parallel to the [***a***,***b***]-plane.

In the following sections, the surface topography of crystals with different habits will be discussed.

3.2. Lozenges

AFM studies of the ultrathin lozenges of Fig. 1d showed reasonably smooth basal {0 0 1} faces. Neither steps nor growth hillocks were detected with AFM, which means that no step generating defects

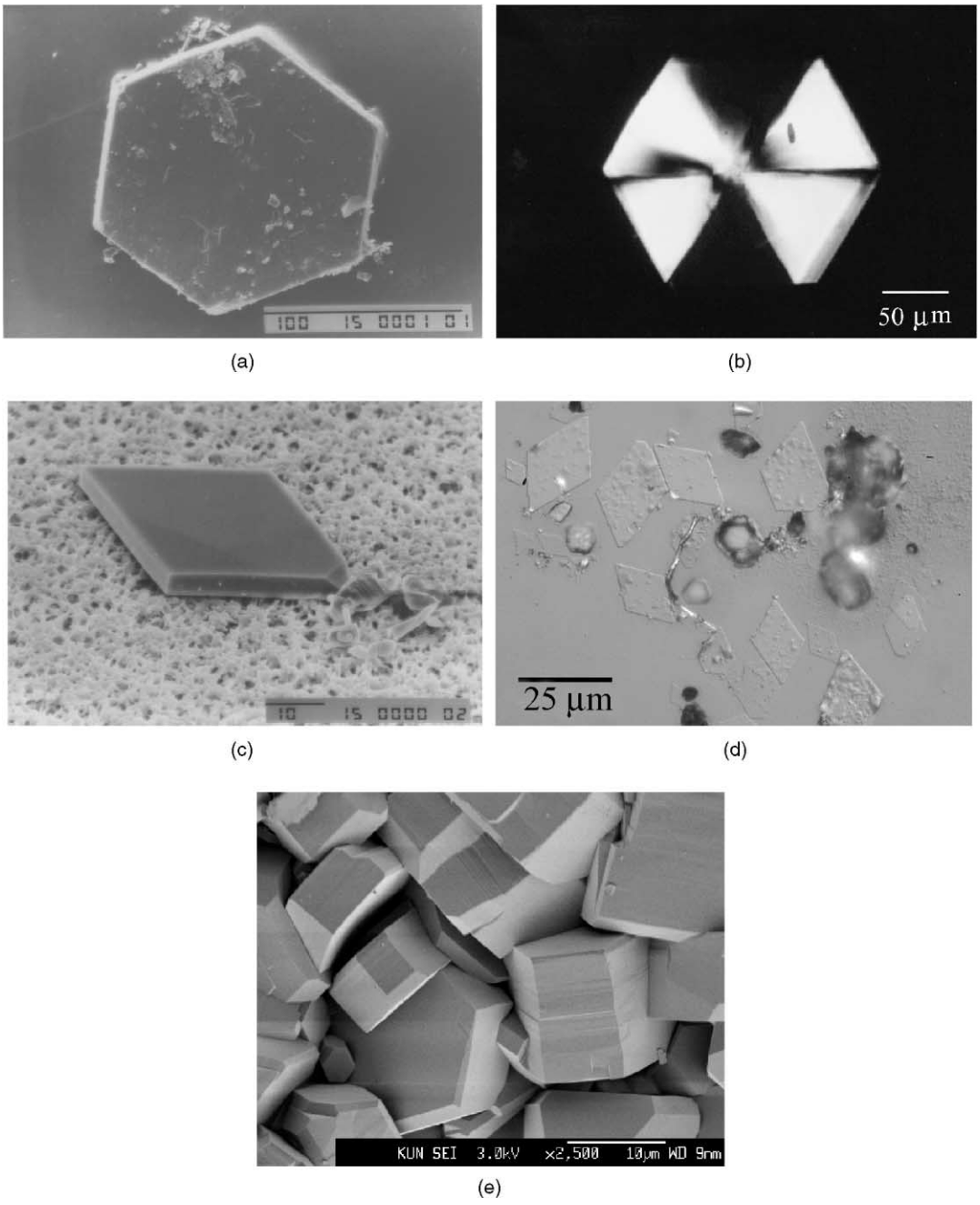

Fig. 1. Micrographs of different crystal morphologies of gibbsite, γ-$Al(OH)_3$: (a) SEM image (scale bar is 100 μm) [24] and (b) optical polarisation micrograph of a sixfold twinned hexagon [24], (c) SEM image of a thicker lozenge, showing a small {1 0 1} face (scale bar is 10 μm) [24], (d) optical micrograph of ultrathin lozenges, and (e) block-shaped crystals (SEM).

were present. Height measurements revealed that the thickness of these ultrathin lozenges was only 20–50 nm, corresponding to 20–50 unit cells perpendicular to the crystal surface. The lateral sizes were similar to those of the other crystals. The aspect ratio of these crystals is >1000 and is the result of the extremely small growth rate of the {0 0 1} faces compared to that of the prismatic faces. This is explained by the weak bonding interaction along the crystallographic *c*-direction between adjacent layers in the packing of the gibbsite structure. The bonding between these layers consists only of hydrogen bonds, while within the layers stronger Al–O covalent/ionic interactions are present. Because of the strong bonds within each layer and the weak association between successive layers, the step free energy on the {0 0 1} is high and, hence, the 2D nucleation rate face is extremely low.

It was not possible to determine the exact orientation of the {1 1 *l*} side faces of the ultrathin lozenges. For thicker lozenges, the prismatic faces were determined to be {1 1 0}. Therefore, the side faces of the ultrathin lozenges are believed to be {1 1 0} as well. Very often the thin lozenges were truncated with unknown faces in the {1 0 *l*} zone. The relative occurrence of these side faces indicates that the growth rate ratio of {1 0 *l*} and {1 1 *l*}, i.e. $R_{\{1\,0\,l\}}/R_{\{1\,1\,l\}}$, is at least 2.

Many of the *thicker* lozenges (5–7 μm thickness, aspect ratio 4–10) showed weakly bunched steps on the basal face, which originate from a growth hillock near the centre of the crystal. Typical examples of such growth hillocks are given in Figs. 2a and b. In Fig. 2b, also some defects can be observed which led to a distortion of the habit. Fig. 2c shows the basic pattern of the growth hillocks, reconstructed from many micrographs of growth hillocks on lozenge-shaped crystals. The growth hillocks have straight steps along two of the ⟨1 1 0⟩ directions, i.e. [1 1 0] and [1 $\bar{1}$ 0] in the region A of Fig. 2c. The steps in opposite directions, i.e. [$\bar{1}\,\bar{1}$ 0] and [$\bar{1}$ 1 0] in region B, are more rounded. The angle between the two ridges separating the region A from B is mostly somewhat less than 120°. This results from a two times larger step propagation velocity in region B as compared to that in region A. The growth hillocks had very small terrace widths, i.e. far beyond the resolution of the optical microscope used, and therefore only some bunched steps could be detected with optical microscopy. Occasionally, a weak ridge was detected in region B, separating the rounded steps roughly parallel to [$\bar{1}\,\bar{1}$ 0] and [$\bar{1}$ 1 0]. The symmetry of the growth hillocks is conform the space group symmetry of the gibbsite structure $P2_1/n$, which means that the 2D point group of the {0 0 1} face is *m*, with its mirror plane perpendicular to ***b***. It is likely that the growth hillocks on the thicker lozenges are composed of a step train generated by a central screw dislocation. This leads to spiral growth and explains the enhanced thickness growth as compared to the ultrathin lozenges which grow by a slow 2D nucleation mechanism.

Detailed observation of the basal face of the thicker lozenges revealed a rough surface on a nanometre scale (Fig. 3). The roughness was caused by hemispherical particles or 2D nuclei which varied from a few nanometres to 50 nm in diameter. Their height was 1–10 nm. The particles did not adsorb preferentially at specific sites, but appeared to be randomly distributed on the terraces. These particles could have been introduced during separation of the crystals from the mother liquor, i.e. due to a shut-off effect. Another possible explanation can be the overlapping plates as observed by Lloyd et al. [21]. These features should then be the spreading {0 0 1} plates acting as a growth mechanism. However, the present AFM micrographs as in Fig. 3 show hemispherical particles with a habit very different from the overlapping plates observed by Lloyd et al. Another possibility to explain the surface roughness observed is a continuous birth and spread mechanism as suggested by Freij et al. [22]. Then this 2D nucleation mechanism occurs simultaneously with the dislocation growth mechanism mentioned above. Although the origin of these 2D and/or 3D particles is not clear, their random distribution points to a shut-off effect as their cause.

The prismatic faces, {1 1 0} and {1 0 0} of the lozenges, were too small to be examined by optical microscopy or AFM. Using SEM, most of the faces showed surfaces which were relatively flawless. Neither steps nor hillocks were detected on these thin faces. However, it must be realised that SEM is not capable of detecting steps lower than a few nanometres. It is not probable, that for the ultrathin lozenges the growth of these faces is dominated by a spiral growth mechanism, as for geometrical reasons

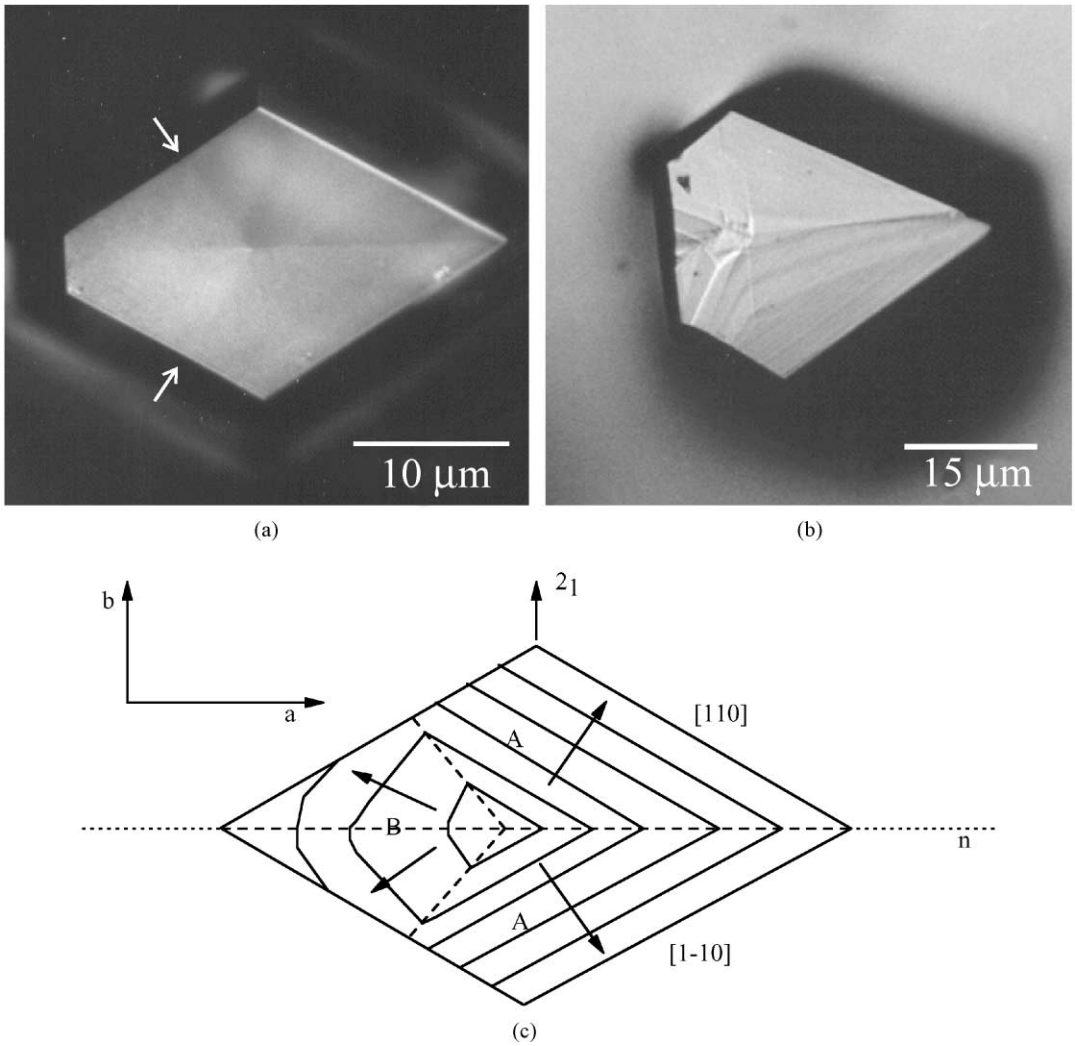

Fig. 2. (a, b) Growth hillocks on thicker lozenge-shaped gibbsite crystals imaged with DICM. In (a), the ridges of the growth hillock can be seen; very low steps are present which were undetectable with optical microscopy. In (b), some weakly bunched steps can be seen. Defects led to the distortion of the crystal. (c) Schematic presentation of step movement from growth hillocks on lozenges. The step propagation directions are indicated by arrows and the ridges of the growth hillock are indicated by dashed lines. The symmetry elements of the space group $P2_1/n$ are also indicated. The areas A and B are referred to in the text.

the screw dislocations would leave these surfaces during growth. Therefore, it is likely that these planes grew by a 2D nucleation mechanism. Moreover, the thicker lozenges have similar lateral sizes as the ultrathin lozenges, suggesting that the prismatic faces of these thicker lozenges grow by the same 2D nucleation mechanism.

According to surface energy calculations, the equilibrium shape of single gibbsite crystals should be hexagonal [29]. However, additional modelling by Fleming et al. [30] showed that for higher caustic concentrations the various crystal faces are covered by different amounts of sodium 'defects'. This leads to changes in surface energy and thus can explain the formation of the observed lozenge (diamond) morphologies of the single crystals. In a forthcoming paper, the growth morphology of gibbsite is explained using an extended connected net analysis [31].

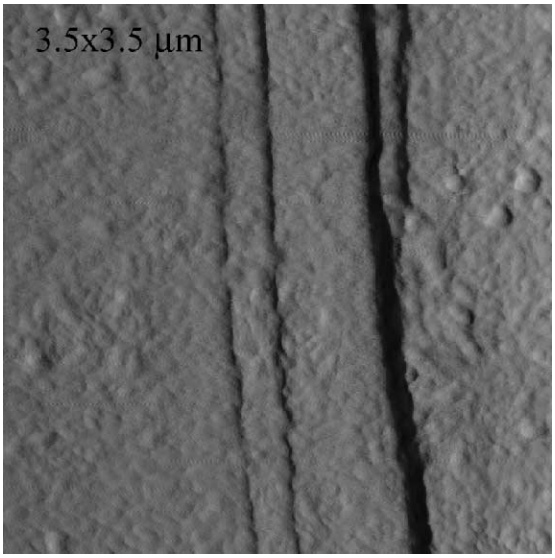

Fig. 3. Hemispherical particles or 2D nuclei which appeared on the basal {0 0 1} face of lozenge-shaped gibbsite crystals (AFM).

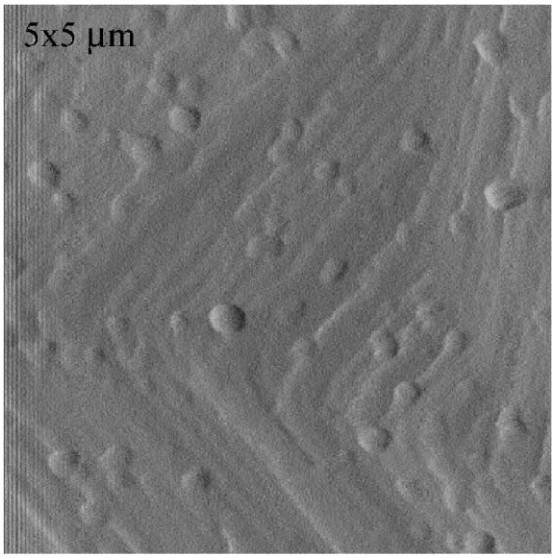

Fig. 4. Very low steps, observed on the {0 0 1} basal face of hexagonal gibbsite crystals (AFM).

3.3. Hexagons

Most of the surface topographic observations described in this paper were obtained from the {0 0 1} basal faces of the relatively large, hexagonal, twinned crystals. The large size of these faces made them more accessible for investigation. The surface morphology of these {0 0 1} faces strongly deviated from the lozenge-shaped crystals described above. Some observations of the prismatic {1 0 0} faces will also be described in this section.

3.3.1. Step patterns

Step patterns on the {0 0 1} faces were briefly discussed in the previous section, where straight steps were found to be present on lozenges along two ⟨1 1 0⟩ directions, and rounded steps were observed to propagate in opposite directions. Similar, but also different patterns were observed on the twinned hexagons.

Very low steps were detected on the {0 0 1} basal faces. In Fig. 4, very low straight steps imaged by AFM are shown. They were present on relatively smooth parts of the {0 0 1} basal faces. The height of these steps was about 0.4 nm, which is half the size of the unit cell along the *c*-axis. This means that the gibbsite surface grows with $d_{0\,0\,2}$ layers, corresponding to single AB stacking layers, in accordance with the selection rule $l = 2n$ for {0 0 l} for the monoclinic space group $P2_1/n$. Often, two of those low steps collided and formed a double growth step, i.e. $d_{\{0\,0\,1\}}$, with a height of about 0.9 nm, equal to the unit cell dimension. Furthermore, macro-steps were commonly observed on the {0 0 1} crystal surfaces. Fig. 5a gives an example of such steps on the {0 0 1} faces. Here, the crystals are part of an agglomerate. The surface shows straight macro-steps along the ⟨1 1 0⟩ and ⟨1 0 0⟩ directions. Both step directions, ⟨1 1 0⟩ and ⟨1 0 0⟩, correspond to periodic bond chain (PBC) directions, which are strong bonding directions in the crystal structure [31]. The ⟨1 1 0⟩ steps were, in general, the most prominent ones. The height of the macro-steps ranged from a few unit cells to hundreds of nanometres and in a few cases to one or a few micrometres.

Fig. 5b shows characteristic macro-step patterns which were observed on the convex top face of perfectly twinned hexagons. Macro-steps emanated from the edge of the crystal and, more specific, from the corner of a particular twin domain. They were oriented at an angle of $30 \pm 10^\circ$ relative to the {1 0 0} side faces. This suggests that the direction of these

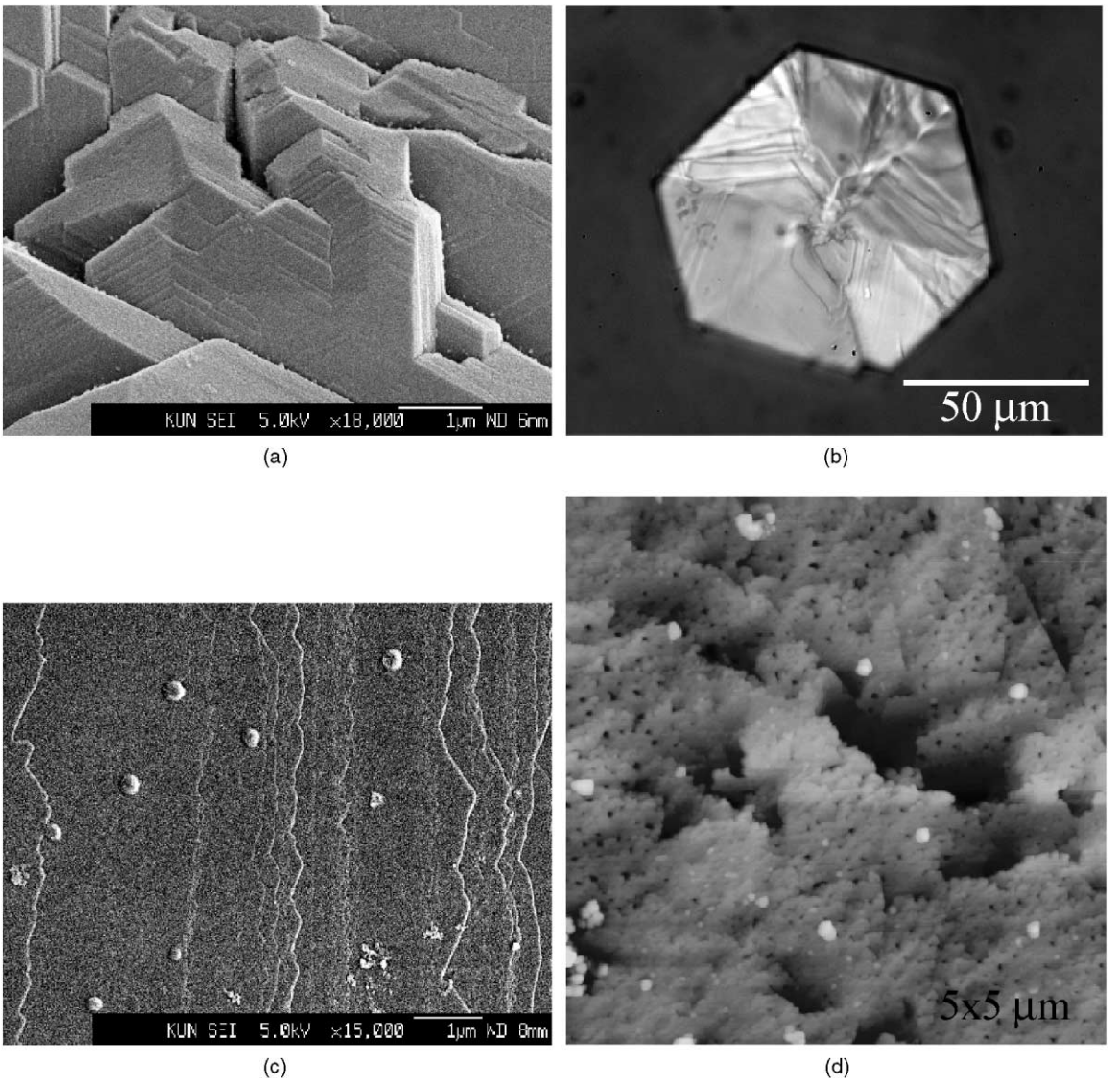

Fig. 5. Step patterns on hexagonal sixfold twinned gibbsite crystals: (a) agglomerate showing bunched step patterns on the {0 0 1} basal face with ⟨1 1 0⟩ and ⟨1 0 0⟩ steps (SEM), (b) optical image of typical ⟨1 3 0⟩ step patterns on the convex top face of a perfectly sixfold twinned gibbsite hexagon, (c) ⟨1 3 0⟩ steps composed of small ⟨1 1 0⟩ and sometimes ⟨1 0 0⟩ steps (SEM), and (d) steps blocked by impurities (AFM).

steps is ⟨1 3 0⟩, which is a—somewhat less stable—PBC direction in the monoclinic gibbsite structure [31]. Closer examination of these ⟨1 3 0⟩ macro-steps using SEM revealed that they were zigzag-shaped, being composed of parts of ⟨1 1 0⟩ and sometimes ⟨1 0 0⟩ steps (Fig. 5c). Lower steps in the ⟨1 3 0⟩-direction were more rounded and showed many cusps, but also these steps were composed of ⟨1 1 0⟩ step segments. In most cases, the ⟨1 3 0⟩ steps changed their overall growth direction when passing a twin boundary, and again obtained an overall ⟨1 3 0⟩-direction on the next crystal domain.

As was observed for the lozenges, also the basal faces of the hexagons were usually rough on a nanometre scale as a result of small hemispherical particles and/or 2D nuclei. Large particles, more than tens of

nanometres in height, were superimposed on the step trains as step decoration or randomly lying on the surface. Smaller particles or 2D nuclei, less than 10 nm in diameter, were also observed. As was discussed in the previous section, these particles are probably the result of a shut-off effect.

In addition, impurity hindering or blocking of steps was observed on surfaces of some batches (Fig. 5d). The shape of these steps is quite rough. This suggests that the impurities adsorbed on the terraces are almost immobile and disturb the step motion, as predicted by Cabrera and Vermileya [32] and van Enckevort and van den Berg [33].

3.3.2. Growth hillocks

The typically shaped growth hillocks found on the thicker lozenges were also observed on the basal face of many twinned hexagons. Examples are shown in Figs. 6a and b. The centre of such a hillock with low step height is shown in Fig. 6c. The average step height as deduced from this AFM micrograph is 0.47 nm, which again corresponds to half a unit cell. It is not possible to verify whether the steps follow a spiral pattern, due to a minimal shut-off effect. In many cases also rounded growth hillocks with very low step heights were observed on the basal gibbsite surfaces.

A second group of growth hillocks was observed, which have their growth centre in the vicinity of another crystal or at the crystal edge as is shown in Figs. 6d and e. These hillocks were very steep with straight, bunched steps in the $\langle 1\,1\,0\rangle$-direction. The inclination of these elevations is about 23°, which is about seven times the slope of the shallow growth hillocks on the lozenges and hexagons, described above. This suggests that here growth has not been introduced by a single dislocation but apparently by a group of dislocations or by intense 2D contact nucleation on edges induced by contacting crystallites. Judged from the steepness of these hillocks, the mechanism must be very effective. Furthermore, it was observed that the steep growth hillocks were capable of passing a twin boundary without changing step direction or step height.

Contact nucleation of growth steps was often observed in the case of an agglomerate. Here the contact point or line of two adjacent crystals acted as a step source by lowering the activation barrier for 2D nucleation (Fig. 7).

3.3.3. Crystallites

On the basal faces of the twinned hexagons, many small crystallites were found to adhere on the surface, especially near the centre (Figs. 8a and b). The thickness of the crystals varied from tens of nanometres to several hundreds of nanometres. Occasionally, the crystallites adsorbed had a height of several micrometres. The crystallites had the characteristic hexagonal and lozenge shapes for gibbsite. The possible origin of these crystallites might be from small clusters in the solution, which have transformed into a crystalline state upon interaction with the lattice of the underlying mother crystal and then are grown to well-faceted crystallites. It is also possible that small gibbsite crystallites formed by 3D nucleation floated in the liquid and sedimented onto the surfaces of the crystals. This phenomenon has recently been observed directly using AFM during the growth of protein crystals [34,35]. Most crystallites were misoriented with respect to the mother crystal. In other cases, their orientation with the underlying mother crystal was more or less the same with respect to the crystallographic ***a*** and ***b*** directions, which suggests reorientation during formation or deposition.

Many of the crystallites were incorporated into the mother crystal. This can be explained by a difference in growth rate between the crystallites and the underlying mother crystal. The small crystallites probably continued to grow after adsorption on the surfaces, but with a smaller growth rate as compared to the mother crystal. This can be explained by the larger number of defects in the mother crystal and, consequently, its larger probability to have step sources of higher strength. In a forthcoming paper, it will be shown that the larger gibbsite crystals indeed possess more defects than smaller crystals [36].

Sometimes, clefts were formed around the misoriented crystallites as a consequence of the growing mother crystal. In other cases, the crystallites were overgrown without clefts, which introduced low-angle grain boundaries if the crystallites were misaligned. These low-angle grain boundaries could become step sources themselves. This category of faults did not deeply penetrate the bulk crystal. Large crystallites on

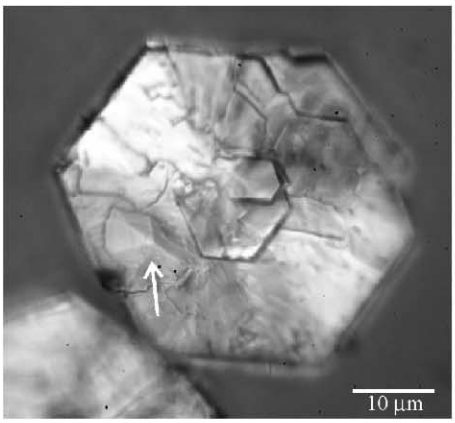

(a)

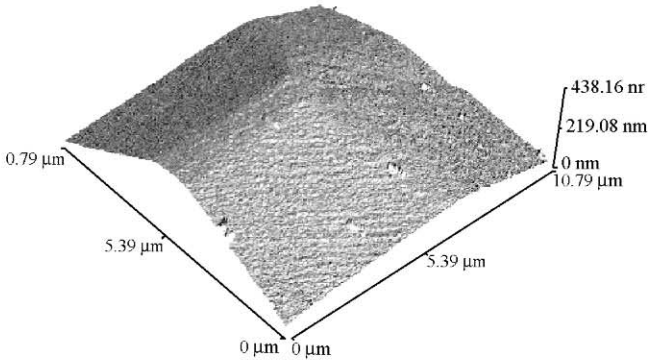

(b)

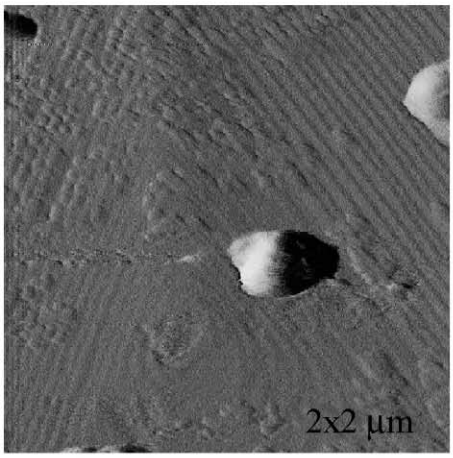

(c)

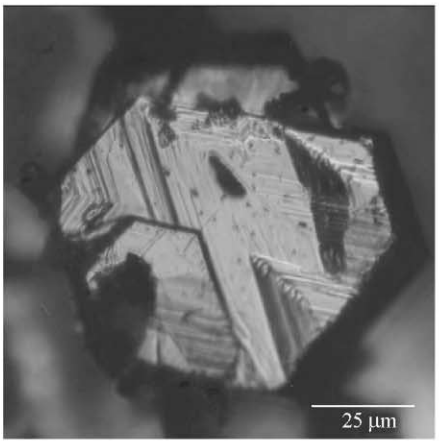

(d)

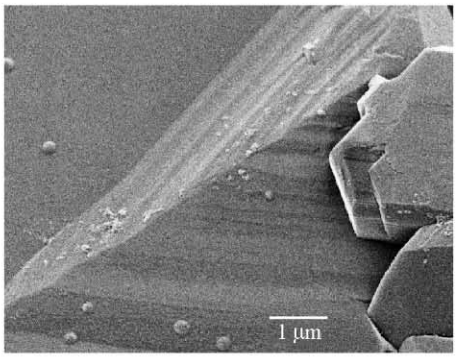

(e)

Fig. 6. Growth hillocks on the basal face of hexagonal sixfold twinned gibbsite crystals: (a) optical micrograph of a triangularly shaped growth hillock indicated by an arrow, (b) AFM topograph of a triangularly shaped growth hillock, (c) step pattern of a growth hillock (AFM), the step height is 0.47 nm, (d) large, steep growth centres in the vicinity of the crystal edge (DICM), and (e) detail of a growth centre of the type as shown in (e) (SEM).

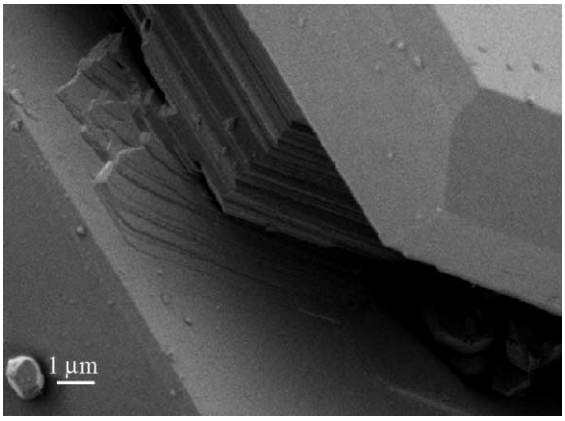

Fig. 7. Steps generated by contact nucleation (SEM).

the basal face could also serve as step sources by contact nucleation.

3.3.4. Planar faults

Planar faults in gibbsite were found as striations on the basal face of the crystals. They are strictly parallel to the crystallographic ⟨1 1 0⟩ and ⟨1 0 0⟩ directions and penetrated the crystal deeply, as was verified using stress birefringence optical microscopy. It was shown that these planar faults continued through the crystal, perpendicular to the basal face within a few degrees. Fig. 8b shows a part of a sixfold twinned hexagon with the outcrops of many of these planar faults at the {0 0 1} surface as indicated by arrows. Besides these striations, strong line features could be observed which are the result of misoriented microcrystals partly grown-in, as discussed in the previous section. It is clear that also these relatively large grain boundaries have well-defined crystallographic directions.

The defect planes did not generate steps; often steps passed these faults, as is shown in Fig. 8c. This led to a particular bunched pattern, the height of which was about 100 nm. With optical microscopy, it was found that the planar faults indeed sometimes stopped just below the surface, which means that a layer grew over the crystal surface covering the defects just before the end of the crystal growth process.

3.3.5. Twin boundaries: concave and convex

The angle between the basal surfaces of adjacent twin domains of a hexagon is about 178°, instead of 180° for a perfect hexagonal crystal. This generates a very shallow re-entrant corner between the faces on the concave top surface of the hexagons [24]. These and other twin boundaries were not important step sources. Occasionally, 2D nuclei were arranged along a twin boundary. The fact that twin boundaries hardly affect the growth of the basal faces also follows from the fact that many macro-steps passed a twin boundary without changing their growth directions.

The gibbsite crystals that were twinned in a very regular way, often had a convex bottom and concave top face. Several of these twinned crystals possessed different surface features on the concave and the

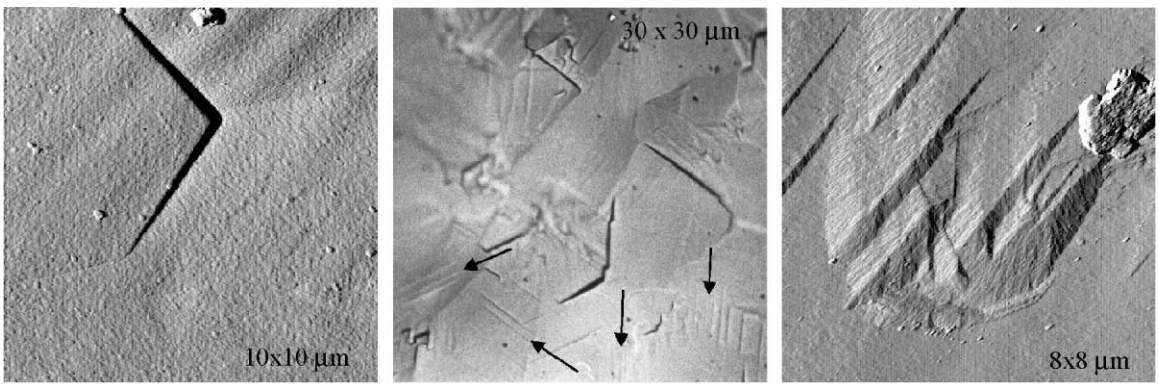

Fig. 8. Planar defects in gibbsite: (a) outcrops of low-angle grain boundaries introduced by a grown-in crystallite on top of a basal face (AFM), (b) stacking faults indicated by arrows (OM), and (c) steps passing stacking faults (AFM), with a step propagation towards the left upper corner.

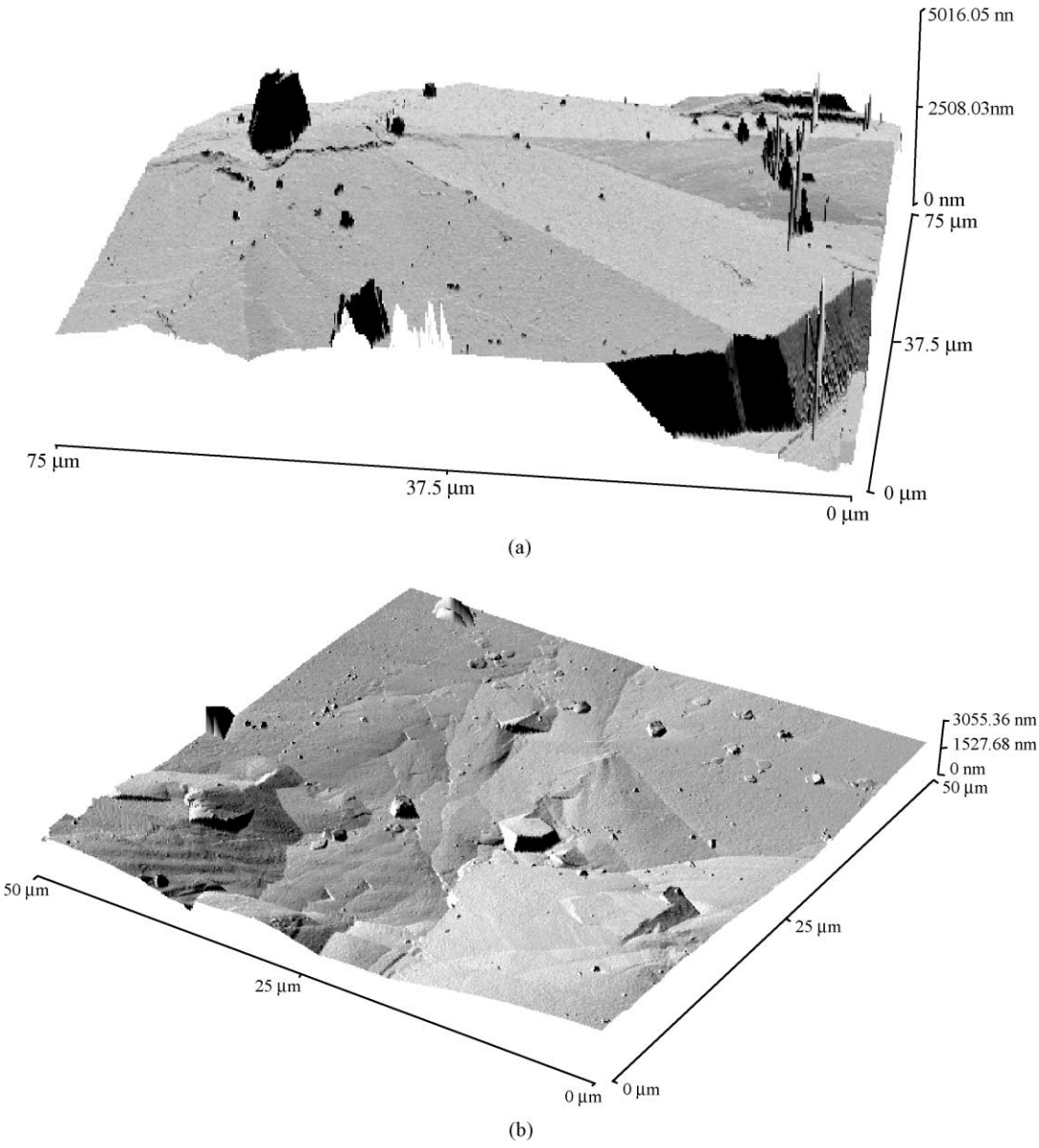

Fig. 9. (a) Convex and (b) concave side of a hexagonal twinned crystal (AFM).

convex crystal sides. The convex side was characterised by straight macro-steps in the ⟨1 1 0⟩ and overall ⟨1 3 0⟩ directions. This side also showed large, more or less polygonised growth hillocks with their centres in the vicinity of the crystal edge. The concave side showed many misoriented crystallites, as elaborated in the previous section, which resulted in a more irregular surface. In addition, the rounded shallow growth hillocks were observed on this side. In Fig. 9, typical AFM images of both the convex and the concave side of a sixfold twinned crystal are shown.

Following the point group 2/*m* as deduced from the space group $P2_1/n$ of the crystals, the two opposite surfaces (0 0 1) and $(0\,0\,\overline{1})$ should exhibit an identical morphology. Therefore, the observations suggest the

occurrence of hypomorphism, or more specific the absence of the twofold axis, as was also found for $K_2Cr_2O_7$ crystals [37] and $NH_4H_2PO_4$ [38]. On the other hand, the concave side of sixfold twinned crystals contains shallow re-entrant corners between adjacent crystal domains. Therefore, 2D nuclei are expected to be preferentially formed on these faces more easily than on the convex faces. In the latter case, the hypomorphism is explained as the result of twinning. The differences between the surface characteristics of the two opposite sides of the twinned crystals were not always clear. No differences were found for the opposite {0 0 1} faces of the lozenge-shaped crystals.

3.3.6. Prismatic faces

The {1 0 0} side faces of the sixfold twinned hexagons sometimes appeared relatively flawless, but were mostly characterised by a striated structure (Fig. 10a). The thickness of the layers varied from less than 50 nm up to a few microns. No steps were observed on these areas; moreover, they appeared rather rough. The striations can be the outcrops of planar faults, like stacking faults or multiple twinning perpendicular to ***c***. Furthermore, the deposition and subsequent lateral growth of a 3D nucleus poorly oriented on the basal face can also result in a slightly misoriented layer and hence in a layer structure. The striations cannot be the result of growth bands due to a non-uniform incorporation of impurities during growth. Then the striations should not be visible on the side faces, but only on cross-sections of the crystals [39].

In the case that the striations are the outcrops of stacking faults, the packing of certain $Al(OH)_3$ layers is according to the bayerite sequence. Sufficiently high densities of stacking faults can be confirmed with XPD. However, the XPD data obtained were similar to the XPD data of gibbsite from the literature [28]. This means that the density of the planar faults was too small, the packing was not according to the bayerite sequence, or the literature XPD data are based on gibbsite crystals highly striated as well.

In the case that the striations are due to the existence of twin lamellae perpendicular to ***c***, it can be detected using polarisation microscopy with crossed polarisers. However, no dark and bright lamellae were revealed, which was possibly due to the 'small' thickness, i.e. less than the resolution of the optical microscope, of the layers.

The occurrence of a 3D (or 2D) nucleus poorly oriented on the basal face, leading to a poorly oriented layer by lateral growth, is shown in Fig. 10b. Here, the upper part of the 'crystal sandwich' has a slightly different orientation than the lower part.

Conclusive evidence, whether these layers are formed by stacking faults, multiple twinning or poorly oriented nuclei followed by growth could not be obtained in this study. Many of the side faces also showed a layer structure in the re-entrant corners at the outcrops of the sixfold twin domain boundaries. Some of the re-entrant corners were curved as is shown in

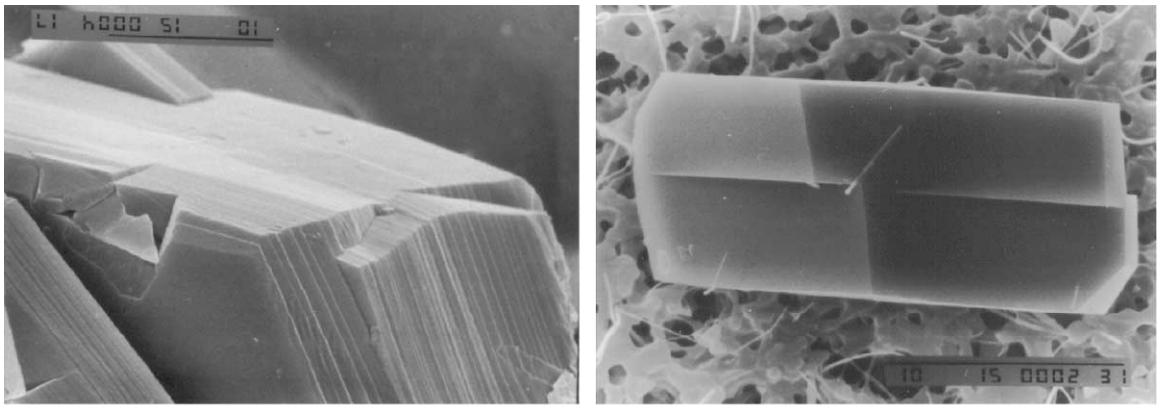

(a) (b)

Fig. 10. SEM images of prismatic faces: (a) prismatic faces with a layered structure (scale bar is 10 μm), and (b) a twist crystal (scale bar is 10 μm).

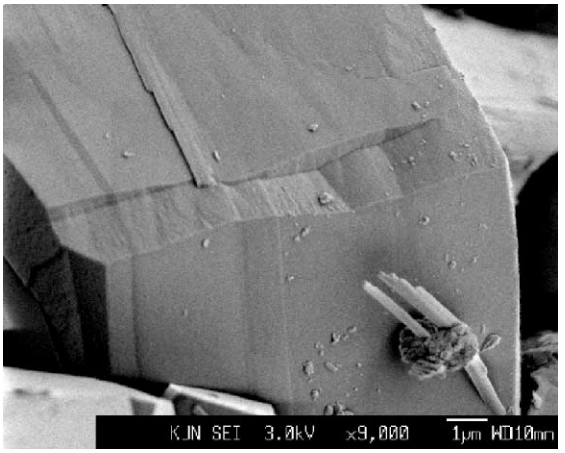

Fig. 11. Curved re-entrant corner as a result of step generation (SEM).

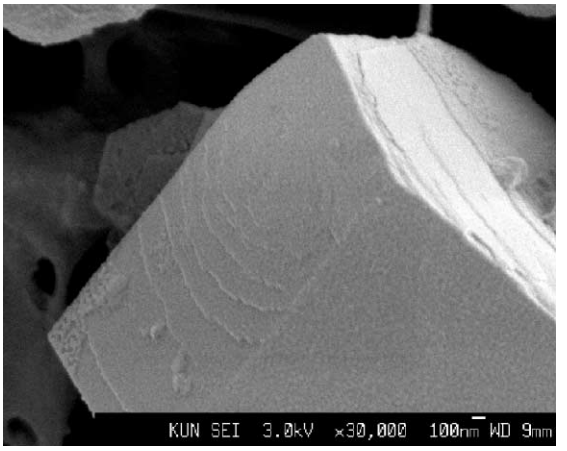

Fig. 12. Step patterns on prismatic face (SEM).

Fig. 11, indicating the activity of the re-entrant corner as a step source. In addition to the striated structure, several hexagonal sixfold twinned crystals showed a planar fault parallel to {0 0 1} traversing the crystal halfway between top and bottom faces. It is likely that these hexagons were mirror twinned perpendicular to the *c*-axis at the early nucleation stage, as was described for prisms in Ref. [24] and in Section 3.4. This mirror twinning could not be confirmed with polarisation microscopy, since it was too difficult to view these crystals from their side face. It was also not possible to verify this mirror twinning by examining the basal face as in this observation direction the two separate domains have the same extinction direction. Hexagons with such a twin boundary did not have the clear layer structure as shown in Fig. 10a, suggesting that here the multiple planar faults did not occur.

3.4. Prisms

The different growth characteristics, which are described above for the lozenges and hexagons, were mostly also observed on the block-like and prismatic gibbsite crystals. On the basal {0 0 1} faces of the prisms, also straight macro-steps parallel to one of the crystallographic directions ⟨1 1 0⟩ or ⟨1 0 0⟩ were observed. Step growth at growth hillocks and generated by contact nucleation were also imaged on these faces. Overgrown crystallites were occasionally observed. These features were revealed with optical microscopy and SEM. AFM was not used, because the prisms were too small to handle for examination.

Most of the prismatic surfaces showed striations parallel to the basal face, in a similar way as for the twinned hexagons. Steps were never observed on the striated structures. Occasionally macro-steps were found on non-striated prismatic surface areas. An example is shown in Fig. 12. The steps are curved and mainly directed parallel to the basal face. Although the large number of defects as well as the mosaic structure discussed below would suggest that growth of the prismatic faces proceeds by contact

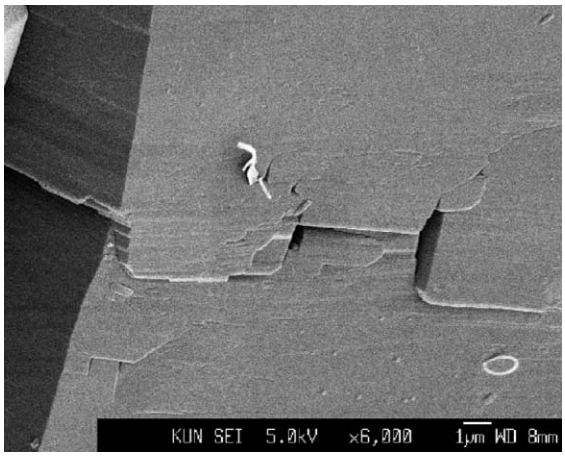

Fig. 13. Block patterns on prismatic faces of a mosaic prism (SEM).

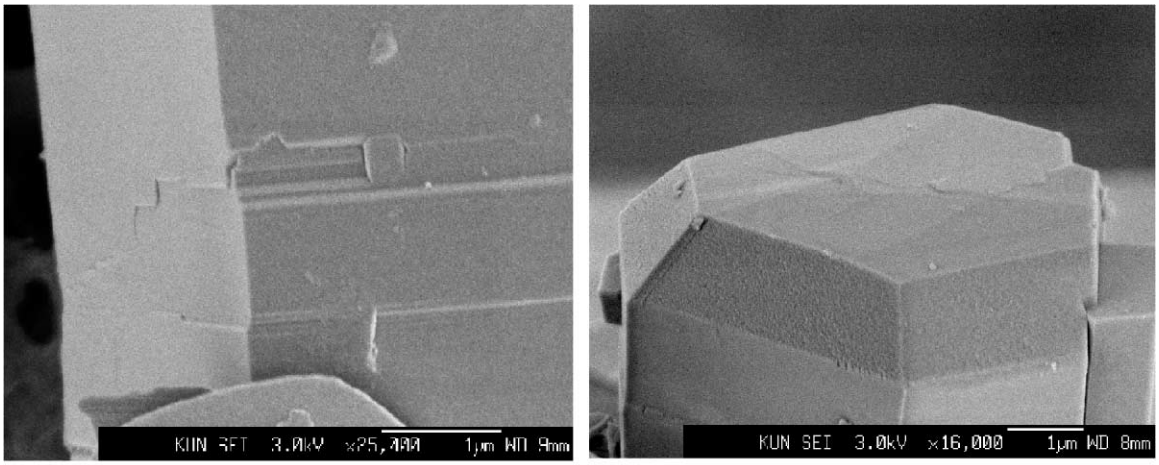

Fig. 14. SEM images of prismatic gibbsite crystals: (a) a mirror twinning along {0 0 1}, and (b) chamfered faces {1 1 2} or {1 0 1}.

nucleation or macro-spirals, steps on these faces were observed in only a few cases. Growth hillocks were not observed. This implies a 2D nucleation growth mechanism. In many cases, protruding block patterns developed on the prismatic surfaces, as is shown in Fig. 13. These block patterns probably reflect a mosaic structure of these gibbsite crystals. Mosaicity and cracks in growing crystals may be caused by stresses resulting from a substantial thermal gradient or the inhomogeneous distribution of point defects [40]. The stress centres induce lattice distortions. Consequently, misfit dislocations will be nucleated and spread in the crystal. In brittle crystals, like gibbsite, where dislocations cannot move, the continuous variations in lattice spacing induced by growth may be resolved by cracking if the crystals grow large enough [40]. Furthermore, the appearance of misoriented 2D or 3D nuclei and the sedimentation of little crystals floating in the liquid onto the surface can also induce cracking, splitting and twisting of the crystals. Since the crystallisation of gibbsite has been performed under isothermal growth conditions, mosaicity is not induced by thermal stresses. A non-uniform distribution of point defects leading to internal stress, dislocations and cracks, the occurrence of misfit 2D and 3D nuclei and the sedimentation of crystallites are more likely to cause the mosaic structure.

Many prisms were inclined along $\boldsymbol{c}$, reflecting a mirror twin perpendicular to the c-axis [24]. In general, the mirror twin was half-way the prism, indicating that twinning occurred during the nucleation stage of gibbsite crystallisation. In Fig. 14a, it is shown that such a twin boundary is not confined to one single plane, but encompasses many layers. Often many adjacent, parallel twin planes led to prismatic faces with numerous inclinations, giving a shallow zigzag pattern. In case that the spacing between the lamellae was very small, this could result in the striated structure as described above.

Some of the prisms had chamfered faces, {1 1 2} and/or {1 0 1} (Fig. 14b). Using high magnification, the surfaces of these facets usually appeared rather rough with very small ($\ll 100$ nm), irregular cone-shaped features parallel to the c-axis. Because of their limited size, these features could not be well resolved with SEM.

It is shown that the prismatic faces of prisms are very often irregular in appearance. The numerous irregularities and the mosaic structure should act as sources for step growth, but steps were only occasionally observed. It is not clear why the growth rate of these irregular faces is not so large that the prisms develop into plate-like crystals. Possibly, the blocking activity of impurities plays a role.

4. Conclusions

In this paper, attention was focused on the surface topography of the three main types of gibbsite crystals—i.e. lozenges, hexagons and prisms—of

which each revealed a different surface structure. Growth of the {0 0 1} basal and {1 1 0} side faces of the ultrathin lozenges proceeds exclusively by 2D nucleation and subsequent step advancement. No dislocation sources were found on any of these lozenges examined. This means that the ultrathin lozenges are the basic growth morphology of gibbsite, and growth is completely determined by 2D nucleation. However, most gibbsite crystals contain many dislocations and other defects. Single crystals with only one or a few screw dislocations ending on the basal face grow to somewhat thicker lozenges. Hexagonal- and block-shaped crystals are sixfold twinned and show a complex surface topography. The different growth features on the {0 0 1} faces, such as step patterns, growth hillocks, planar faults, partly grown-in crystallites and steps generated by contact nucleation are shown to be the result of different defects in the crystals and inhomogeneities in their environment. The lowest steps are about 5 Å high, which is equal to half of the unit cell dimension along ***c*** in accordance with the selection rules of the space group. The surfaces of prismatic faces are characterised by striations parallel to {0 0 1}. These layers are the outcrops of planar faults or slightly misoriented growth layers. Steps sources were not resolved on the prismatic faces, which suggests that growth is according to a 2D nucleation mechanism. In Ref. [24], steps generated at re-entrant corners were mentioned as a source for accelerated growth in lateral direction for twinned crystals. Such steps in re-entrant corners were indeed observed. Mosaicity, observed for many prisms, was related to the presence of impurities or a non-coherent 2D and 3D nucleation mechanism.

In brief, the growth of gibbsite crystals is largely determined by its defect structure, formed during the nucleation phase and during growth. This explains the large variety in habit and size of crystals grown under identical conditions. However, there is still the question why the lateral growth rate of prisms is lower than that of plates and lozenges.

Acknowledgements

Billiton Aluminium B.V. is kindly acknowledged for the financial support and permission to publish this work.

References

[1] C. Misra, E.T. White, J. Cryst. Growth 8 (1971) 172.
[2] W.R. King, Light Met. (1973) 551.
[3] N. Brown, J. Cryst. Growth 29 (1975) 309.
[4] P.J. The, Light Met. (1980) 119.
[5] A. Packter, H. Daill, Cryst. Res. Technol. 17 (1982) 931.
[6] D. Ilievski, E.T. White, Chemeca '90 (1990) 1156.
[7] D. Ilievski, E.T. White, Chem. Eng. Sci. 49 (1994) 3227.
[8] D. Ilievski, E.T. White, AIChE J. 41 (1995) 518.
[9] H. Nagai, S. Hokazono, A. Kato, Br. Ceram. Trans. J. 90 (1991) 44.
[10] S. Veesler, R. Boistelle, J. Cryst. Growth 130 (1993) 411.
[11] S. Veesler, R. Boistelle, J. Cryst. Growth 142 (1994) 177.
[12] S. Kumar, R.G. Bautista, Light Met. (1994) 47.
[13] P.G. Smith, H.R. Watling, P. Crew, Colloid. Surf. A 111 (1996) 119.
[14] I. Seyssiecq, S. Veesler, G. Pèpe, R. Boistelle, J. Cryst. Growth 196 (1999) 174.
[15] I. Seyssiecq, S. Veesler, R. Boistelle, J.M. Lamérant, Chem. Eng. Sci. 53 (1998) 2177.
[16] H.R. Watling, S.D. Fleming, W. van Bronswijk, A.L. Rohl, J. Chem. Soc., Dalton Trans. (1998) 3911.
[17] O.I. Arakelyan, A.A. Chistyakova, Sov. J. Non-Ferrous Met. (1959) 6.
[18] V.A. Derevyankin, S.I. Kuznetsov, Sov. J. Non-Ferrous Met. 2 (1961) 47.
[19] B. Gnyra, R.F. Jooste, N. Brown, J. Cryst. Growth 21 (1974) 141.
[20] N. Brown, J. Cryst. Growth 12 (1972) 39.
[21] S. Lloyd, S.M. Thurgate, R.M. Cornell, G.M. Parkinson, Appl. Surf. Sci. 135 (1998) 178.
[22] S. Freij, M.-Y. Lee, M. Reyhani, G. Parkinson, in: Proceedings of the Fifth International Alumina Quality Workshop, 1999, p. 41.
[23] J. Addai-Mensah, Min. Eng. 10 (1997) 81.
[24] C. Sweegers, H. Meekes, W.J.P. van Enckevort, P. Bennema, I.D.K. Hiralal, A. Rijkeboer, J. Cryst. Growth 197 (1999) 244.
[25] B.N. McCoy, J.L. Dewey, Light Met. (1982) 173.
[26] H. Saalfeld, M. Wedde, Z. für Kristall. 139 (1974) 129.
[27] W.A. Deer, R.A. Howie, J. Zussman, An Introduction to Rock Forming Minerals, 2nd Edition, Longman, New York, 1992.
[28] K. Wefers, C. Misra, Oxides and hydroxides of aluminium (revised), Technical Report Technical Paper No. 19, Alcoa Research Laboratories, Pittsburgh, PA, 1987.
[29] S. Fleming, A. Rohl, M.Y. Lee, J. Gale, G. Parkinson, J. Cryst. Growth 209 (2000) 159.
[30] S.D. Fleming, A.L. Rohl, S.C. Parker, G.M. Parkinson, J. Phys. Chem. B 105 (2001) 5099.
[31] C. Sweegers, S.X.M. Boerrigter, R.F.P. Grimbergen, H. Meekes, S. Fleming, I.D.K. Hiralal, A. Rijkeboer, J. Phys. Chem. B, in press.
[32] N. Cabrera, D.A. Vermileya, in: Growth and Perfection of Crystals, Wiley, New York, 1958, p. 393.
[33] W.J.P. van Enckevort, A.C.J.F. van den Berg, J. Cryst. Growth 183 (1998) 441.

[34] A.J. Malkin, Yu.G. Kuznetsov, A. McPherson, J. Cryst. Growth 196 (1999) 471–488.
[35] J.P. Astier, D. Bokern, L. Lapena, S. Veesler, J. Cryst. Growth 226 (2001) 294–302.
[36] C. Sweegers, H.C. de Coninck, H. Meekes, W.J.P. van Enckevort, I.D.K. Hiralal, A. Rijkeboer, J. Cryst. Growth 233 (2001) 567–582.
[37] A.J. Derksen, W.J.P. van Enckevort, M.S. Couto, J. Phys. D 27 (1994) 2580.
[38] M.A. Verheijen, L.P.J. Vogels, H. Meekes, J. Cryst. Growth 160 (1996) 337.
[39] K. Sangwal, K.W. Benz, Prog. Cryst. Growth Char. Mater. 32 (1996) 135.
[40] A.A. Chernov, J. Cryst. Growth 196 (1999) 524.